Redox paradox of vanadium in Tavorite LiVPO4F1-yOy

Edouard Boivin, Antonella Iadecola, François Fauth, Jean-Noël Chotard, Christian Masquelier, Laurence Croguennec

The redox paradox of Vanadium in Tavorite $LiVPO_4F_{1-y}O_y$.

Edouard Boivin [a,b,c], Antonella Iadecola [c], François Fauth [d],
Jean-Noël Chotard [b,c,e], Christian Masquelier [b,c,e] and Laurence Croguennec [a,c,e,1]

[a] CNRS, Univ. Bordeaux, Bordeaux INP, ICMCB, UMR CNRS 5026, F-33600 Pessac, France.
[b] Laboratoire de Réactivité et de Chimie des Solides, UMR CNRS 7314,
Université de Picardie Jules Verne, F-80039 Amiens Cedex 1, France.
[c] RS2E, Réseau Français sur le Stockage Electrochimique de l'Energie, FR CNRS 3459,
F-80039 Amiens Cedex 1, France.
[d] CELLS - ALBA synchrotron, E-08290 Cerdanyola del Vallès, Barcelona, Spain.
[e] ALISTORE-ERI European Research Institute, FR CNRS 3104, F-80039 Amiens Cedex 1, France.

Abstract:

Vanadyl-type defects in vanadium oxy-fluoride phosphates confer interesting properties to these materials as positive electrodes in Li-ion or Na-ion batteries. The influence of defects concentration on the phase diagram and redox mechanisms in $LiVPO_4F_{1-y}O_y$ Tavorite phases has been investigated by combining *operando* Synchrotron X-ray powder diffraction (SXRPD) and X-ray absorption spectroscopy (XAS). O*perando* X-ray absorption near edge structure (XANES) reveals the activation of the V^{4+}=O/V^{5+}=O redox couple during the first step of the charge, and then upon further Li^+ extraction the activation of the V^{3+}/V^{4+} redox couple in fluorine-rich environments. This result, although surprising, is in full agreement with the operating voltages of the end-member phases, as $Li_xV^{III,IV}PO_4F$ operates at higher voltage than $Li_xV^{IV,V}PO_4O$. The unexpected succession of these redox couples is observed for the first time in the same material. The small volume changes undergone by the materials upon electrochemical operation were proposed to be at the origin of the better performance observed for the mixed valence samples: "freezing" of the framework is observed all along the activation of the V^{4+}=O/V^{5+}=O redox couple in a solid solution type domain.

[1] Corresponding author : L. Croguennec (Laurence.Croguennec@icmcb.cnrs.fr)

Introduction

The increasing mobility of populations and the need to fight against global warming with the development of sustainable energies are two reasons for which electrochemical energy storage is one of the major topics for scientific research, both at the academic and industrial levels. Lithium-ion batteries are already largely used as an energy source for mobile devices such as smartphones, laptops, etc. Nevertheless, for applications such as electric and hybrid vehicles, the energy density delivered by these batteries cannot currently compete with fossil energy (limited autonomy in particular). Polyanionic compounds (phosphates, sulphates) are interesting positive electrode materials for lithium-ion batteries due to the higher working potential for the $M^{n+}/M^{(n+1)+}$ redox couple, in comparison to that observed in oxides [1] and, for some of them, higher chemical and thermal stability[2]. Among them, $LiV^{III}PO_4F$ and $LiV^{IV}PO_4O$ Tavorite-type compounds are competitive with the already commercialized $LiFePO_4$. Indeed, operating on the V^{3+}/V^{4+} redox couple, $LiVPO_4F$ delivers an energy density of 655 Wh/kg [3], whereas $LiVPO_4O$ delivers 615 Wh/kg involving the $V^{4+}=O/V^{5+}=O$ (often called $(VO)^{2+}/(VO)^{3+}$) redox couple [4] (against 586 Wh/kg for $LiFePO_4$ [5]). Moreover, it would be possible to increase the energy density by playing with the ability of vanadium to be stabilized in a large range of oxidation states ($V^{2+}/V^{3+}/V^{4+}/V^{5+}$) although the difference between insertion and extraction voltages might be too high to be exploited for real applications [6]. Kang and coworkers have proposed to reduce this voltage difference by substituting partially O^{2-} for F^- in $LiVPO_4F$ and compositions such as $Li_xVPO_4F_{1-y}O_y$ were shown to deliver ca. 800 Wh/kg in an extended voltage window, with the exchange of 1.6 electrons/vanadium between 2.0 - 4.5 V *vs.* Li^+/Li based on the activation of the V^{3+}/V^{4+} and $V^{4+}=O/V^{5+}=O$ redox couples [7]. However, the activation of $V^{3+}/V^{4+}/V^{5+}$ redox in this material seems to be detrimental to the long life performance, with ~50% of capacity fading after 15 cycles at the cycling rate of C/20 (*i.e.* one charge performed in 20 hours).

Beyond the possibility of multi-electrons systems offered by $LiVPO_4F_{1-y}O_y$ compositions, we have already demonstrated [8] that vanadyl-type defects are valuable for the electrochemical performance of $LiVPO_4F$, in a similar way than the carbon coating or particles' size reduction can be. The in-depth structural description of $LiVPO_4F_{1-y}O_y$ pristine compounds are summarized in **Figure 1,** where both the long range and local structures are provided by XRD and XAS respectively [8].The cationic (*i.e.* V^{3+}/V^{4+}) and anionic (*i.e.* O^{2-}/F^-) distribution along the propagation direction of the chains of vanadium octahedra (*i.e.* [001] direction, see **Figure 1a**) were shown: (i) not to be ordered (no superstructure identified), (ii) to be associated with significant constrains identified through a strong anisotropic broadening of the diffraction lines and (iii) to a significant deviation of the cell parameters from the Vegard's law. Such findings suggest the formation of crystalline domains being locally different in oxygen/fluorine

composition, and thus in vanadyl bond concentration with a strong local impact on the structure. As X-ray diffraction is a long range characterization technique, it allowed for only an average description of centro-symmetric vanadium octahedra (**Figure 1b**). The presence of local vanadyl-type distortions in $LiVPO_4F_{1-y}O_y$ was confirmed thanks to V K-edge XAS experiment, that highlights the occurrence of different $VO_4(F,O)_2$ local environments. The mixed fluorine/oxygen V^{4+} octahedra ($V^{4+}O_4(O_1F_1)$) are shrunk versus the pure oxygen environment for V^{4+}, $V^{4+}O_4(O_1O_1)$, and the V^{3+} octahedral environments $V^{3+}O_4(O,F)_2$ (**Figure 1c**). This leads to an average shortening of the cell parameters related to the propagation direction of the chains of octahedra and would explain the offset from the Vegard's law. This behavior has been assigned to the competition between the ionicity of the V^{3+}-F bond and the covalency of the V^{4+}=O (vanadyl) bond which strongly impacts the crystal field and the configuration of the vanadium's orbitals, and makes difficult their full statistical miscibility. It appears that an optimal vanadyl-type bond concentration exists around y = 0.35 in $LiVPO_4F_{1-y}O_y$, with improved reversible capacity and rate capability compared to the end member phases, $LiVPO_4F$ and $LiVPO_4O$. The phase diagram as well as the redox mechanisms observed during lithium deintercalation from $LiVPO_4F_{1-y}O_y$ have been scrutinized in details and are reported in this paper with special emphasis on the impact of the vanadyl-type bonds concentration.

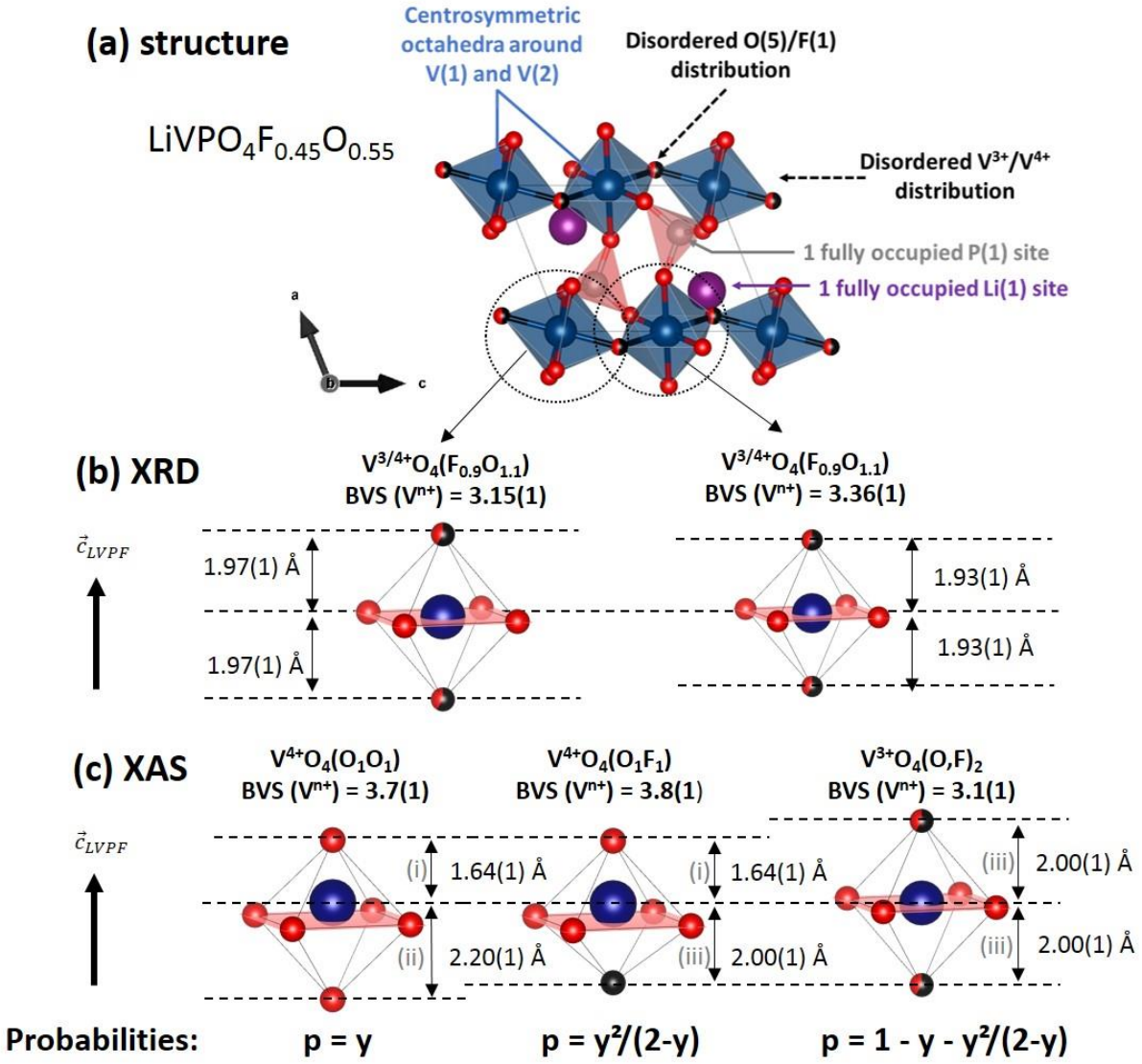

Figure 1: Summary of the structural description of the pristine materials provided in ref. 8. **(a)** The structure of $LiVPO_4F_{0.45}O_{0.55}$ highlighting the disordered cationic (V^{3+}/V^{4+}) and anionic (O^{2-}/F^-) distributions along the chains of octahedra. **(b)** Schematic representation of the environment of the two crystallographically different vanadium sites V(1) and V(2) with their corresponding BVS values. **(c)** The local environments of vanadium observed by XAS with their corresponding BVS values and probability of appearance

Experimental part

Operando synchrotron radiation diffraction measurements were performed at the MSPD beamline[9] of the ALBA synchrotron with an operating wavelength of 0.9535(1) Å. **Figure S1a** given in supplementary information shows the comparison between the patterns of $LiVPO_4F_{0.45}O_{0.55}$ recorded *in situ* (*i.e.* in the electrochemical cell [10]) and in a sealed capillary. The *in situ* pattern contains a series of additional contributions arising from the battery

components and $Li_3V_2(PO_4)_3$ impurity. Indeed, during *operando* experiments performed in transmission mode, the beam is going through all the layers of the battery, generating narrow Bragg peaks from lithium (negative electrode), beryllium (two windows, one on both sides of the cell stacking), and aluminum (current collector), as well as broad contributions from the polytetrafluoroethylene (PTFE) used as binder and from the Whatman separators. The comparison between the two patterns allows identifying the 2θ regions where these additional peaks appear and to exclude them in order to achieve a structural determination of the electrode material during the operando experiment. All the diffraction data collected were thus analyzed by Rietveld refinement in classical or in sequential mode of the Fullprof software[11]. Moreover, due to the setup constraints, the electrode used for this *operando* diffraction experiment had to be self-supported and the use of PTFE as binder was thus preferred with an electrode loading of 70/20/10 (active material/carbon/PTFE). Due to small differences in the electrode loading, the electrochemical signature obtained in the *in situ* cell differs slightly compared to the one obtained in coin cell; **Figure S1b** illustrates these differences. A fully delithiated sample was measured *ex situ*: the self-supported electrode was recovered from a Swagelok cell after cycling at C/200 rate until 4.6 V *vs.* Li^+/Li, washed with dimethyl carbonate (DMC), dried under vacuum, introduced and sealed under Argon in a 0.4 mm diameter capillary.

Operando X-ray absorption spectroscopy measurements were performed at the Vanadium K-edge in transmission mode on the ROCK beamline[12] at SOLEIL synchrotron (France). A Si(111) channel-cut quick-XAS monochromator at 5.5 KeV was used, with an energy resolution of 0.6 eV ($\Delta E/E \approx 10^{-4}$). 0.2 eV was used as energy sampling around the edge position to convert the original nexus data format to the txt one. The intensity of the monochromatic X-ray beam was measured by three consecutive ionization detectors. Self-supported PTFE-based films, whose loading had to be adjusted according to the absorption coefficient (*i.e.* a ratio of 50/45/5 for active material, carbon and PTFE respectively), were used and cycled at C/15 in the potential window 3.0 - 4.45 V *vs.* Li^+/Li. The electrode formulation with a high percentage of carbon leads to a voltage profile close to the one obtained in GITT (Galvanostatic Intermittent Titration Technique) equilibrium conditions (**Figure S1b**, grey dots) whereas the lower capacity and larger polarization obtained in coin cell (blue line) and in the XRD *in situ* cell (black line), is probably due to kinetic limitation induced by a higher loading (80 and 70% of active material). Successive spectra were collected every 15 minutes during 5 minutes leading to 56 spectra. The energy calibration was established with the simultaneous absorption measurement of a vanadium metal foil. The data were treated using the Athena software[13] for the energy calibration and normalization. The XAS data set was used as input for the Principal Component Analysis (PCA), revealing that 3 components were necessary to describe the evolution of the XAS spectra during the charge. Then, the principal components were reconstructed using the multivariate curve resolution–alternating least-squares (MCR-

ALS) analysis[14,15]. Finally, the EXAFS oscillations of the reconstructed components were fitted using the Artemis software[13]. Fourier transforms of the k² weighted EXAFS oscillations were carried out in the k range from 2.7 - 12.7 $Å^{-1}$. Fitting was performed in the R range from 1 – 2.05 Å. EXAFS amplitudes and phase shifts were calculated by FEFF7. Except for the radial distance (R_i) and the Debye–Waller factor (σ_i^2), all the other parameters were kept constant: the coordination number of each V-X bond (N=6 oxygen as O^{2-} and F^- are similar X-ray scatterers), the energy reference shift (E_0=0 eV), and the attenuation factor (S_0^2=1).

Results and discussion

Phase diagram as observed by Synchrotron X-ray powder diffraction

Figure 2a shows the SXRPD patterns recorded *operando* during lithium extraction from $LiVPO_4F_{0.45}O_{0.55}$ and that of the fully delithiated composition $VPO_4F_{0.45}O_{0.55}$ obtained *ex situ*. As suggested by the electrochemical data given in **Figure S1b** (blue line), the full delithiation isn't achieved *operando*. Indeed, the last pattern recorded corresponds to the composition $Li_{\sim 0.2}VPO_4F_{0.45}O_{0.55}$ and appears obviously significantly different from the one obtained *ex situ* for the fully delithiated material. However, already at this state of charge, the end member $VPO_4F_{0.45}O_{0.55}$ could be identified and had thus started to grow in a two-phase region. Indeed, as shown in **Figure 2b** that compares the patterns of the specific compositions $LiVPO_4F_{0.45}O_{0.55}$, $Li_{0.75}VPO_4F_{0.45}O_{0.55}$, $Li_{0.45}VPO_4F_{0.45}O_{0.55}$, $Li_{0.35}VPO_4F_{0.45}O_{0.55}$, $Li_{0.25}VPO_4F_{0.45}O_{0.55}$ and $VPO_4F_{0.45}O_{0.55}$, the most intense peaks characteristic of $VPO_4F_{0.45}O_{0.55}$ are detected, for instance at 2θ = 17.7°. Except from the peaks associated to the minor impurity ($Li_{3-x}V_2(PO_4)_3$) and to the contributions from the *in situ* cell (Lithium, Beryllium, Aluminum, PTFE and separator), no additional peaks have been detected suggesting that no Lithium/vacancy ordering takes place within the tunnels of the Tavorite structure.

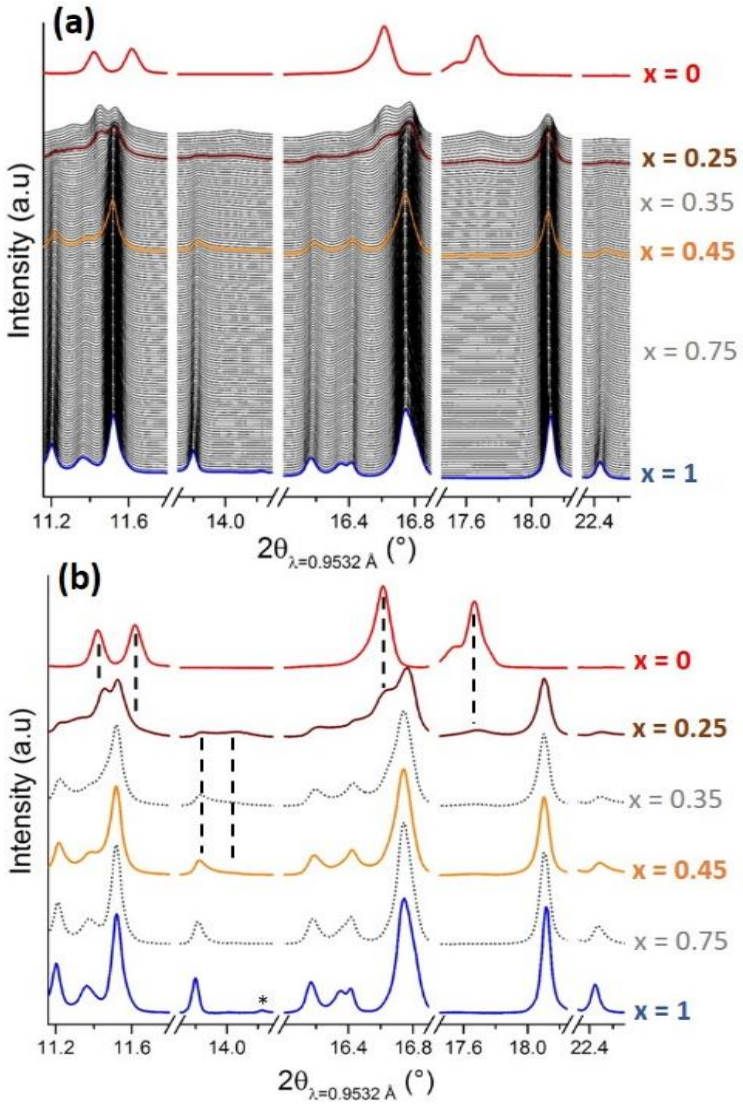

Figure 2: **(a)** SXRPD patterns obtained *operando* during lithium extraction from $LiVPO_4F_{0.45}O_{0.55}$. The material corresponding to the red pattern has been obtained *ex situ*. **(b)** Selected SXRPD patterns at specific compositions. At the very beginning of the charge, the Bragg peaks related to the electrochemically active $Li_3V_2(PO_4)_3$ impurity disappear (as highlighted at 14.3° by *)[16]. This is in good agreement with the small shoulders seen on the voltage profile at 3.7 and 4.1V *vs.* Li^+/Li on charge (as shown in Figure S1b).

During the removal of the first 0.55 Li^+, anisotropic weak shifts of the initial Bragg peaks were observed together with the appearance of a second minor phase. The *a* and *b* parameters of the main phase slightly decrease (0.13 and 0.08% respectively) while the *c* parameter slightly increases (0.23%), leading to a very small unit-cell volume change for $Li_xVPO_4F_{0.45}O_{0.55}$ (0.03% for the exchange of 0.55 electrons, see **Figure 3a**). The results of the Rietveld refinement performed for $LiVPO_4F_{0.45}O_{0.55}$ and $Li_{0.45}VPO_4F_{0.45}O_{0.55}$ are compared in **Figure S2** and **Table S1** in supplementary information. The two structures appear to be very similar, as expected for the two end members of a $LiVPO_4F_{0.45}O_{0.55}$ - $Li_{0.45}VPO_4F_{0.45}O_{0.55}$ solid solution. The single lithium site would be continuously emptied and characterized by Li-O

distances ranging between 1.93(4) Å and 2.25(3) Å for $Li_{0.45}VPO_4F_{0.45}O_{0.55}$ *vs.* 1.88(4) Å and 2.31(3) Å for $LiVPO_4F_{0.45}O_{0.55}$, the V-X distances along the chains remaining constant (from 1.952(9) Å to 1.953(9) Å in average on the two vanadium sites).

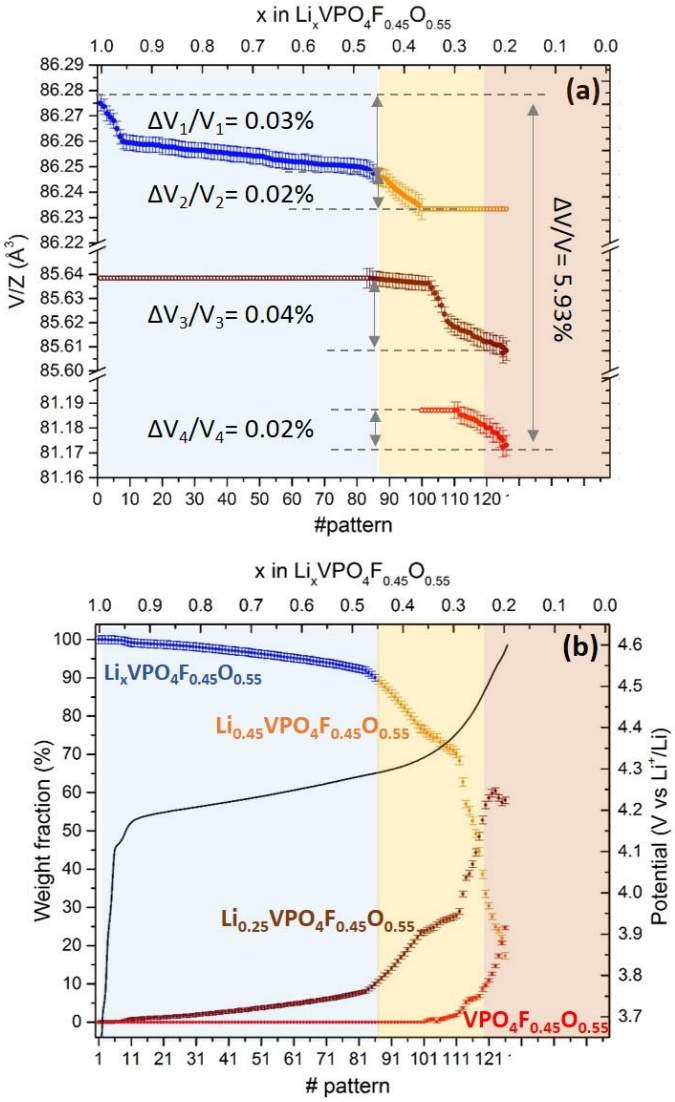

Figure 3: Evolution of the cell volumes **(a)** and weight fractions **(b)** of the phases appearing along the reaction path. For (b) the values without error bar are associated to refinement with fixed cell parameters. The three domains are identified: a solid solution one for $Li_xVPO_4F_{0.45}O_{0.55}$ ($0.45 \leq x \leq 1$) in blue, an apparent biphasic domain in orange between $Li_{0.45}VPO_4F_{0.45}O_{0.55}$ and $Li_{0.25}VPO_4F_{0.45}O_{0.55}$, and a second apparent biphasic domain between $Li_{0.25}VPO_4F_{0.45}O_{0.55}$ and $VPO_4F_{0.45}O_{0.55}$.

Further delithiation leads to the disappearance of the $Li_{0.45}VPO_4F_{0.45}O_{0.55}$ phase according to a pseudo-biphasic mechanism, as highlighted in **Figure 2b**, at the benefit of the $Li_{0.25}VPO_4F_{0.45}O_{0.55}$ one which has a significantly smaller cell volume, as shown in **Figure 3a**. The Rietveld refinement of $Li_{0.25}VPO_4F_{0.45}O_{0.55}$ is not trivial due to: (i) the presence of two additional phases next to it, the first being $Li_{0.45}VPO_4F_{0.55}O_{0.45}$ and the second one identified as $VPO_4F_{0.55}O_{0.45}$ by comparison with the composition obtained *ex situ* (see **Figure S3** and **Table S2** in supplementary information), (ii) the strong anisotropic broadening of the

diffraction lines and (iii) the small amount of Li^+ ions remaining in the structure which doesn't allow to determine their position. Nevertheless, V-X distances along the chains could be determined to be of 1.946(7) Å in $Li_{0.25}VPO_4F_{0.45}O_{0.55}$.

As the full delithiation was not achieved *operando* despite the appearance of $VPO_4F_{0.45}O_{0.55}$ at the very end of the experiment, the SXRPD pattern of the fully delithiated material was recorded from a sample prepared *ex situ* in a standard electrochemical cell in conditions theoretically close to the equilibrium (10 µA/cm², at a rate of C/200). Despite these soft electrochemical lithium extraction conditions, the SXRPD pattern reveals a complex line profile with a strong anisotropic broadening that can be taken into account considering - next to the main "phase" - a secondary "phase" whose most easily identified diffraction lines would be at 16.2, 16.6, 17.9 and 30.0° (as highlighted by arrows in inset of **Figure 4a**). As shown in **Figure 4b**, the experimental pattern could be explained considering the presence of two $VPO_4F_{1-y}O_y$ and $VPO_4F_{1-y'}O_{y'}$ "phases" (see **Table S3** for more information). The composition of these two "phases" could be estimated to be close to the major $VPO_4F_{0.43}O_{0.57}$ for $VPO_4F_{1-y}O_y$, and to minor $VPO_4F_{0.24}O_{0.76}$ for $VPO_4F_{1-y'}O_{y'}$ from the linear variation of the V/Z values determined from the end members VPO_4F and VPO_4O (*i.e.* 80.42(1) $Å^3$ and 81.98(1) $Å^3$ respectively [16,17]). The first one is characterized by a cell volume such as V/Z is equal to 81.09(1) $Å^3$, whereas the second one is characterized by a V/Z of 81.60(8) $Å^3$. The description of the end member by two phases does not mean that we assume a phase separation during the lithium deintercalation reaction, or even the presence of extended crystalline domains that we could have not identified for the pristine materials. These two "phases" are in fact associated to local domains of slightly different average compositions, one being richer in fluorine and thus in ionic V^{4+}-F bonds and the other being richer in oxygen and thus in covalent V^{5+}=O bonds. Locally, at the interface between the two types of domains, strains are observed due to the competition between these ionic and covalent bonds around vanadium atoms. These strains are less obvious, and thus less observed, for the pristine compositions as the difference in cell volumes is only 1.9% between $LiVPO_4F$ and $LiVPO_4O$ whereas it is 2.8% between their fully deintercalated counterparts. The Rietveld refinement of the structure of the main "phase" $VPO4F_{1-y}O_y$ was performed considering the VPO_4F-type model described in the *C2/c* space group (**Figure 4**)[18], with constant distances along the chains (d(V-X) = 1.94(1) Å), whereas the structure of the minor "phase" $VPO_4F_{1-y'}O_{y'}$ was performed within the *Cc* space group, similar to that used to describe VPO_4O, allowing an alternation between a short bond and a longer bond along the chains of octahedra.

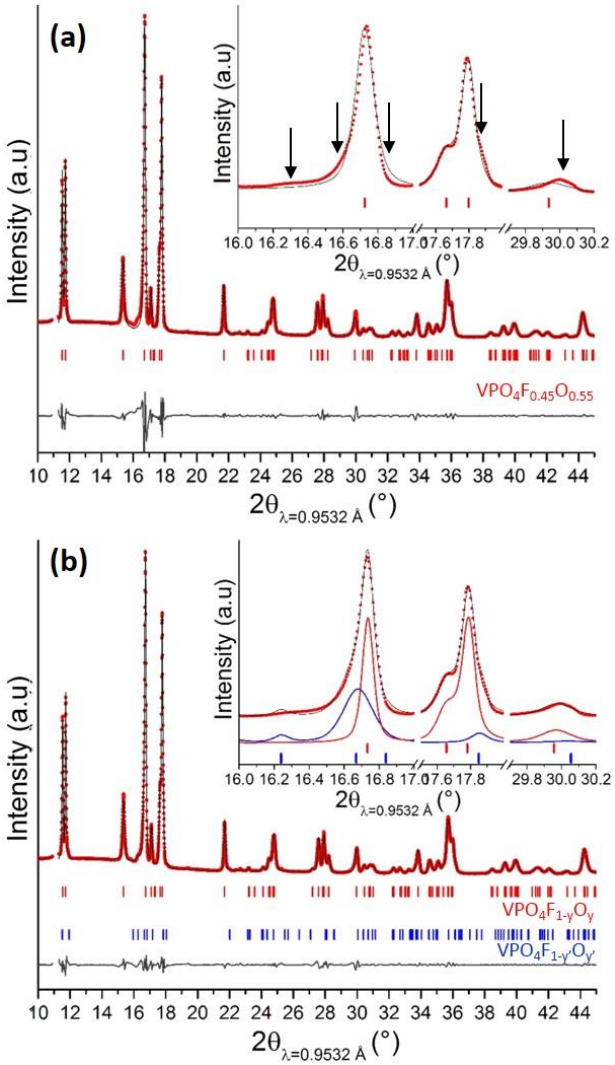

***Figure 4**: Rietveld refinements performed for the composition $VPO_4F_{0.45}O_{0.55}$: **(a)** considering a single phase described in the C2/c space group and **(b)** considering the contribution of two "phases", the major one $VPO_4F_{1-y}O_y$ and the minor one $VPO_4F_{1-y'}O_{y'}$, the latter being described in the Cc space group. The corresponding Bragg positions are plotted as red and blue marks, respectively.*

The evolution of the weight fractions of the intermediate phases identified during the deintercalation process is given in **Figure 3b**. This figure reveals, among others, that the extraction mechanisms (monophasic or biphasic) cannot be clearly defined. Indeed, during the "apparent biphasic processes", the volume change observed for each phase is in the same order of magnitude than that measured during the monophasic mechanism. The disordered O^{2-}/F^- distribution in the starting phase induces local inhomogeneous delithiation, in relationship with the local composition being either rich in oxygen or rich in fluorine. This phenomenon is seen, in average, as a combination between monophasic and biphasic reactions whereas it could actually correspond to a multitude of successive local biphasic reactions out of the equilibrium state.

Similar *operando* SXRPD experiments were performed for two other compositions, $LiVPO_4F_{0.35}O_{0.65}$ and $LiVPO_4F_{0.25}O_{0.75}$, in order to investigate the influence of the vanadyl-type defects' concentration on the phase diagrams observed during lithium extraction. The diffraction patterns obtained for $LiVPO_4F_{0.25}O_{0.75}$ are given as example in **Figure S4**, and **Figure 5** summarizes the phase diagrams obtained for five different compounds $LiVPO_4F_{1-y}O_y$ (y = 0, 0.35, 0.55, 0.75 and 1).

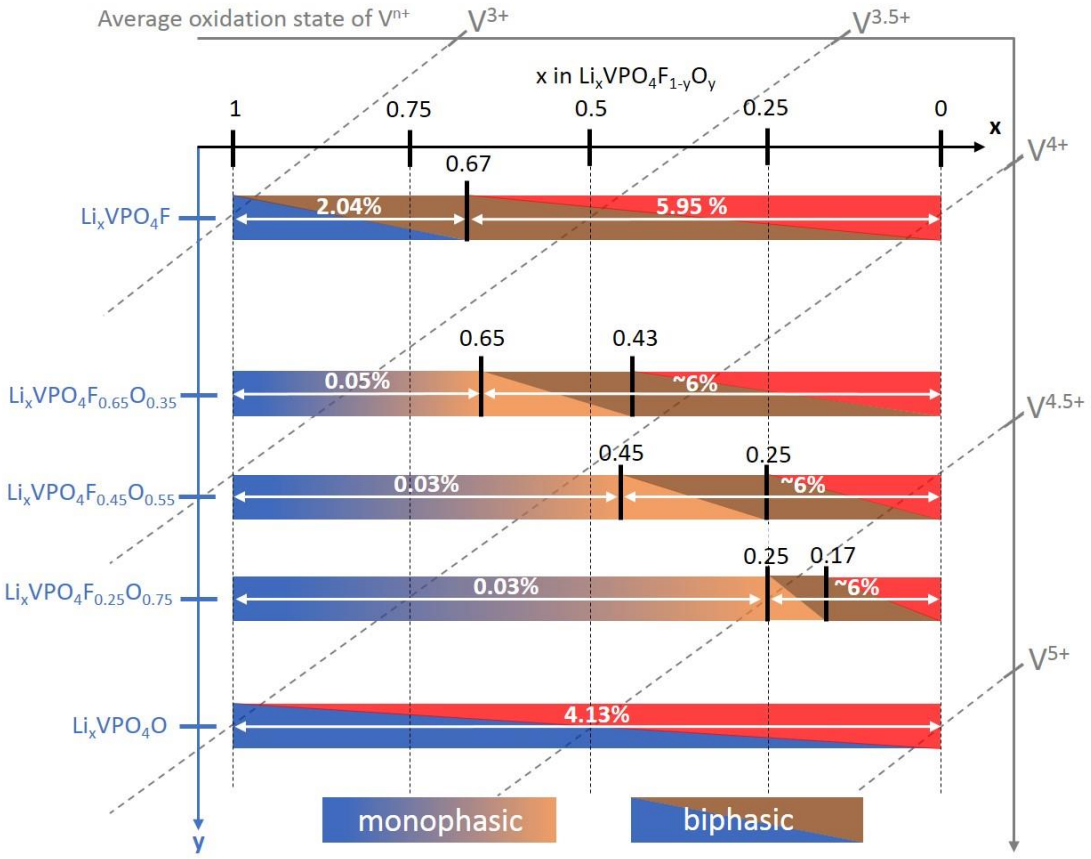

Figure 5: Schematic phase diagrams observed by X-ray diffraction for the $Li_xVPO_4F_{1-y}O_y$ system. The "demixing/strains effect" observed at the end of the charge isn't represented. The diagonal lines represent the average oxidation state of vanadium in the material. The volume variations are also reported in %.

They reveal a similar structural evolution with an apparent solid solution process at the beginning of the charge for $0 < y < 1$, whose composition domain depends on the amount of V^{4+} in the starting material. Indeed, this mechanism is observed in $Li_xVPO_4F_{1-y}O_y$ for $1 \geq x \geq 0.25$, $1 \geq x \geq 0.45$ and $1 \geq x \geq 0.65$ for y = 0.75, y = 0.55 and y = 0.35 respectively, i.e. until $\Delta x = y$. Therefore, it could correspond to the activation of the V^{4+}=O/V^{5+}=O redox couple, before the activation of the V^{3+}/V^{4+} redox couple in vanadyl-free environments ($V^{3+}O_4F_2$ or $V^{3+}O_4FO$). Moreover, as observed for $Li_xVPO_4F_{0.45}O_{0.55}$, the structural changes observed during this monophasic process are very small. **Figure S5** compares the volume changes ($\Delta V/V$) as a

function of the state of charge for the three samples studied: ca. +0.03%, -0.03% and -0.05% for y = 0.75, 0.55 and 0.35 in $Li_xVPO_4F_{1-y}O_y$ respectively. The subsequent lithium deintercalation occurs according to two consecutive pseudo biphasic processes involving the intermediate phases for x ~ 0.17 in $Li_xVPO_4F_{0.25}O_{0.75}$ and x ~ 0.43 in $Li_xVPO_4F_{0.65}O_{0.35}$ as highlighted in **Figure 5**. This phase transition seems to present some similarities with the one observed at the $Li_{0.67}VPO_4F$ composition for $LiVPO_4F$. Indeed, whatever the oxidation state of vanadium in the starting material, the phase transition appears at a V^{3+}/V^{4+} ratio approximately equal to 2. Nevertheless, even using bright SXRPD source, we weren't able to identify the superstructure peaks observed in the $Li_{0.67}VPO_4F$ [19] phase for the $Li_xVPO_4F_{1-y}O_y$ samples. Its limitation to the local rich-fluorine domains makes it much more difficult to be detected.

The partial substitution of oxygen for fluorine in $LiVPO_4F_{1-y}O_y$ leads to smaller volume changes along the lithium extraction compared to the ones observed for the Li_xVPO_4F[16] (~6% *vs.* 8.0%), but remains higher to the one observed for Li_xVPO_4O (*i.e.* 4.1%)[17]. Although smaller volume changes are observed upon electrochemical cycling for $LiVPO_4O$, the local structural modifications involved by the oxidation of V^{4+}=O to V^{5+}=O are strong, from a distorted vanadium octahedron to a pyramid with an elongation of the "anti-vanadyl" V^{5+}--O bond and shortening of the V-O bonds belonging to the square plane. The weaker structural changes for the $Li_xVPO_4F_{1-y}O_y$ samples compared to the end-member phases (Li_xVPO_4F, Li_xVPO_4O) seem to be at the origin of their improved electrochemical performance. Moreover, as (i) the structure seems to be frozen during the first step of the lithium deintercalation reaction (*i.e.* within the solid solution domain until $\Delta x = y$ in $Li_xVPO_4F_{1-y}O_y$) and (ii) the further lithium deintercalation to reach the fully delithiated state leads to similar volume changes (~6%) whatever the F^-/O^{2-} substitution ratio, the vanadyl-type bonds' concentration for optimized electrochemical performance could arise from the balance between these two processes (i) and (ii). Indeed, for oxygen-rich materials (characterized by a wide solid solution domain) the structure undergoes major structural modifications in a narrow composition range ($\Delta V/V$ ~6% for Δx = 0.25 in $Li_xVPO_4F_{0.25}O_{0.75}$) whereas for the fluorine-rich materials (showing a narrow solid solution domain), these changes are spread on a large composition range ($\Delta V/V$ ~6% for Δx = 0.65 in $Li_xVPO_4F_{0.65}O_{0.35}$). For the latter, softer structural changes are observed and they could be at the origin of the better rate capability and cycling stability of fluorine-rich solid solutions materials[8].

Operando SXRPD allowed to get an overall picture of the structural modifications upon charge occurring in $LiVPO_4F_{1-y}O_y$ as positive electrode materials in lithium batteries. In the case of a disordered O^{2-}/F^- distribution and considering the lightness of lithium, the description of the phases obtained during lithium deintercalation is only partial. However, the identification

of the composition domains successively observed allows to make hypotheses about the redox mechanisms: activation of the V^{4+}=O/V^{5+}=O redox couple in the monophasic domains and of the V^{3+}/V^{4+} redox couple during the following biphasic reactions. A close inspection of the redox mechanisms and of the local environmental changes around vanadium was done using XAS in order to get a thorough understanding of these phenomena.

The redox paradox around vanadium

Operando XAS spectra were recorded at V K-edge during the charge of the Li // $LiVPO_4F_{0.45}O_{0.55}$ cell in the 3.0 - 4.45 V *vs.* Li^+/Li voltage range (**Figure 6a**). The vanadium K-edge XANES spectrum of the pristine material exhibits several features. The main absorption edge corresponds to the 1s → 4p dipole-allowed transition. Its rather linear shift towards higher energies from $LiVPO_4F_{0.45}O_{0.55}$ to $VPO_4F_{0.45}O_{0.55}$ (*i.e.* from 5481.9 to 5484.9 eV at half jump, **Figure S6a**) is consistent with an increase of the vanadium oxidation state during the charge. The weaker pre-edge contribution located between 5465 and 5473 eV (inset of **Figure 6a**) arises from the theoretically forbidden 1s to 3d transition which becomes allowed due to the distortion of the local environment around vanadium (*i.e.* vanadyl-type distortion). The assignment of the pre-edge peaks is complex and some Tavorite-type references were required: we ascribe the peak observed at 5468.0 eV to V^{3+} (as for $LiV^{III}PO_4F$), at 5469.2 and 5470.7 eV to V^{4+}=O and V^{5+}=O contributions respectively (as shown in **Figure S7b** for $LiV^{IV}PO_4O$ and $V^{V}PO_4O$).

The parallel evolution of the pre-edge intensity and of the edge position is reported in **Figure S6a**. The position of the edge shifts almost linearly during the oxidation of vanadium whereas the global pre-edge intensity increases strongly until the spectrum 31 (*i.e.* $Li_{0.45}VPO_4F_{0.45}O_{0.55}$) and then stagnates. This evolution suggests that the whole set of data cannot be described as a simple linear combination of the initial and final spectra. Therefore, the complete data set was analyzed using Principal Component Analysis (PCA) combined with multivariate curves resolution alternating least-squares method (MCR-ALS)[14,15] as previously used in similar other operando XAS studies[20,21]. The variance plot obtained from PCA (**Figure S6b**) indicates that about 99.74% of the variance of the XAS spectra can be described using the combination of three principal components. Although *operando* SXRPD has identified at least 4 distinct phases required to describe the phase diagram observed upon Lithium extraction, the addition of a fourth component would only explain 0.05% and could constitute

an over interpretation of the signal. Therefore, the residual part has been considered as the experimental noise.

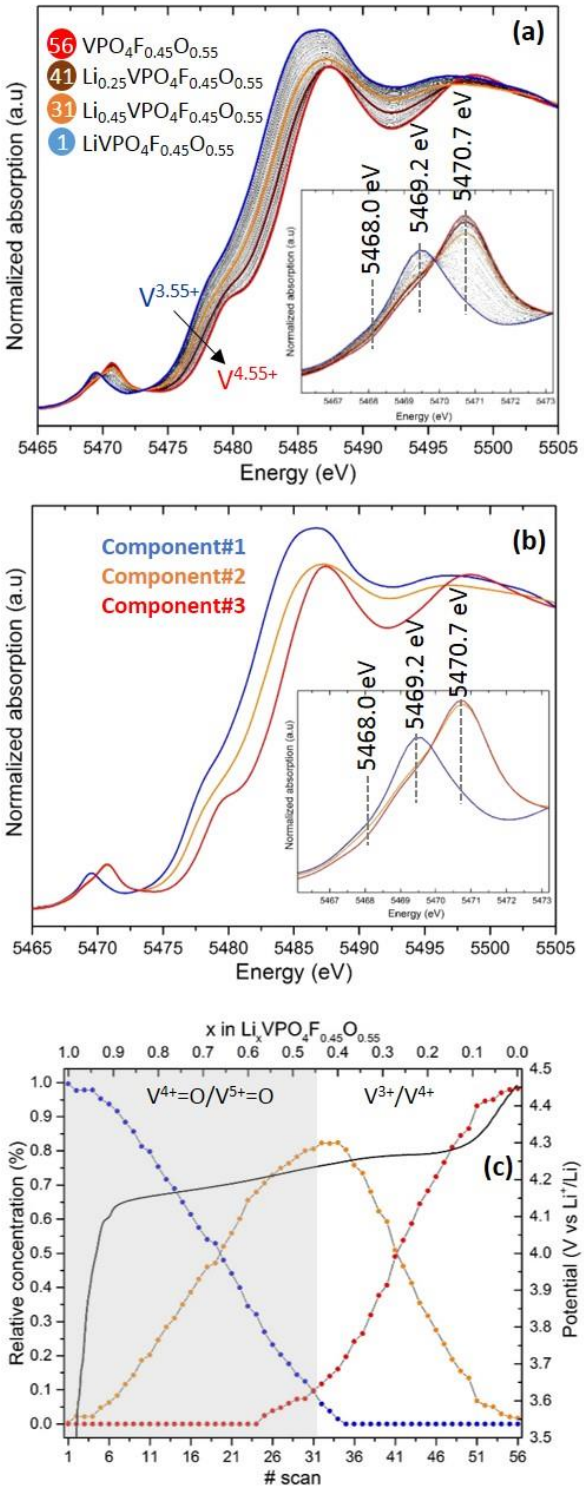

Figure 6: (a) V K-edge XANES spectra recorded during charge of $LiVPO_4F_{0.45}O_{0.55}$ and in inset the enlargement of the pre-edge region. The colored spectra (#1, #31, #41 and #56) correspond to the specific compositions obtained by SXRPD experiment. (b) The reconstructed components obtained using MCR-ALS analysis. (c) The evolution of the relative amount of each component as a function of the scan number is superimposed to the voltage profile obtained during the operando experiment (black line).

The three reconstructed components are displayed in **Figure 6b** with the evolution of their relative amount along the electrochemical reaction in **Figure 6c**. These components can be described as follows: component#1 corresponds to the pristine material $LiVPO_4F_{0.45}O_{0.55}$ and component#3 to the fully delithiated one $VPO_4F_{0.45}O_{0.55}$. Since component#2 never reaches 100% of the relative amount, it cannot be identified with an experimental spectrum. However, as its maximum contribution corresponds to the $Li_{0.45}VPO_4F_{0.45}O_{0.55}$ composition, this component can be assigned to the phase identified at the end of the solid solution domain observed by *operando* SXRPD (*i.e.* when $\Delta x = y$ in $Li_xVPO_4F_{1-y}O_y$). Comparing the absorption energy for each component, it evolves linearly as a function of the oxidation state of vanadium. The pre-edges of the reconstructed components show three main contributions observed at 5468.0, 5469.2 and 5470.7 eV with different relative intensities along lithium extraction. Between component#1 and component#2, the decrease of the V^{4+}=O contribution (*i.e.* 5469.2 eV) is clearly accompanied by an increase of the V^{5+}=O contribution (*i.e.* 5470.7 eV), revealing the activation of the V^{4+}=O/V^{5+}=O redox couple during the first part of the lithium extraction as suggested by *operando* SXRPD. For component#3, a slight decrease of the V^{3+} contribution (*i.e.* 5468.0 eV) is observed, with in fact almost no modification of the pre-edge versus that observed for the component#2.

Therefore, the V^{3+}/V^{4+} redox couple seems to be activated at higher voltage compared to the V^{4+}=O/V^{5+}=O one, leading to the formation of a mixed valence V^{3+}/V^{5+} phase at the end of the first vanadium oxidation step (*i.e.* $Li_{0.45}(V^{3+}_{0.45}V^{5+}_{0.55})PO_4F_{0.45}O_{0.55}$). This result, although surprising, is in full agreement with the operating voltages of the end-member phases. Indeed, the V^{4+}=O/V^{5+}=O redox couple is observed in Li_xVPO_4O at a lower potential than the V^{3+}/V^{4+} redox couple in Li_xVPO_4F (*i.e.* 3.95 V for V^{4+}=O/V^{5+}=O in Li_xVPO_4O and 4.24 V for V^{3+}/V^{4+} in Li_xVPO_4F)[3]: the covalency of the vanadyl bond acts as a “reverse inductive effect”, decreasing significantly the potential of the V^{4+}=O/V^{5+}=O redox couple.

The local structure as a support of the proposed redox mechanism

The Fourier transforms of k^2-weighted EXAFS spectra of the reconstructed components and their corresponding fits are given in **Figure S8**. The model used to describe the starting material, already reported in ref. 8, is built on 3 populations of bonds around vanadium with different probabilities depending on the F^-/O^{2-} substitution ratio (*i.e.* y in $LiVPO_4F_{1-y}O_y$). During electrochemical cycling, new environments are expected to be generated. Thus, an additional degree of freedom has been considered to fit separately the bond lengths belonging to the square plane of the octahedra (i.e. (iv) in **Figure 7** and **Table S4**) and those being perpendicular

(i.e. (i), (ii) and/or (iii) in **Figure 7** and **Table S4**). Therefore, we assumed a 6-fold coordination for vanadium with the following constraints:

(i) the number of V^{n+}=O (n > 3) vanadyl bonds was fixed to the number of V^{4+} in the starting material,

(ii) the "anti-vanadyl" V^{4+}--O and V^{5+}--O bonds are formed only by vanadium involved in a vanadyl bond and having an oxygen as antagonist ligand,

(iii) all other V^{n+}-X bonds along the propagation direction of the octahedra have been considered to be equivalent,

(iv) all the V^{n+}-O bonds (with n = 3, 4 or 5) belonging to the square plane of VO_4X_2 have also been considered to be equivalent.

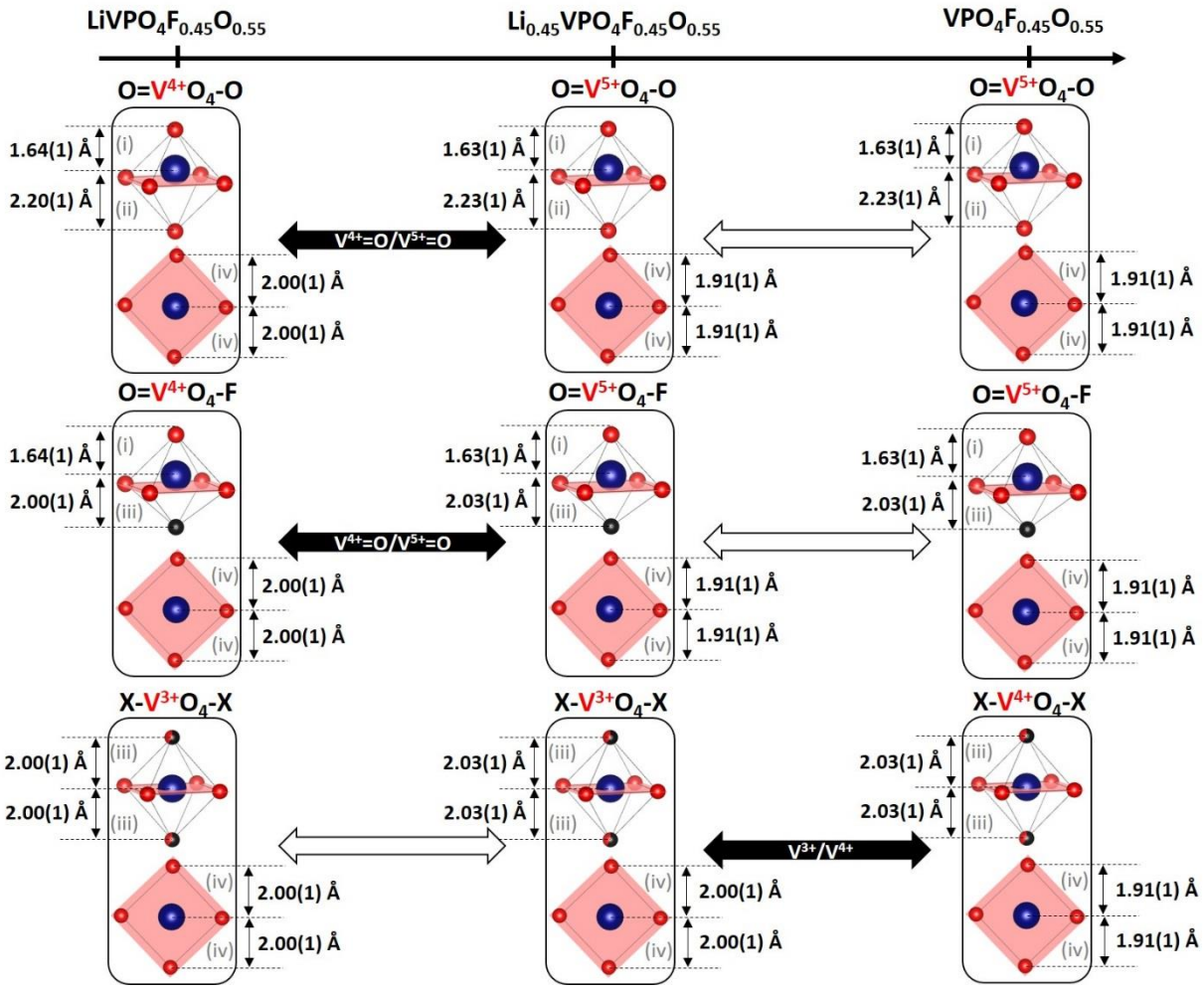

Figure 7: Schematic representation of the evolution of the local environments around vanadium upon electrochemical cycling. The starting material, $LiVPO_4F_{0.45}O_{0.55}$, contains 3 different vanadium environments ($O=V^{4+}O_4$-O, $O=V^{4+}O_4$-F and X-$V^{3+}O_4$-X, represented from the top to the bottom) characterized by 4 kinds of bond distances: (i), (ii), (iii) and (iv) (see text) evolving upon Li extraction (from the left to the right). The redox couples involved during each step are mentioned in the black arrows while the white arrows indicates the absence of electrochemical activity.

This leads to 5 parameters to refine (4 different populations of bond lengths and a common Debye Waller factor for all of them) for 7 independent parameters ($2.\Delta k.\Delta R/\pi \sim 7$). For the composition studied, $LiVPO_4F_{0.45}O_{0.55}$, the coordination [0.55 + 0.20 + 1.25 + 4] for (i) vanadyl V^{4+}=O, (ii) "anti-vanadyl" V^{4+}--O , (iii) apical V^{n+}-X and (iv) equatorial V^{n+}-O respectively has been used. This model provides, for the fit of the component#1, a similar description than the model provided in ref. 8 : the vanadyl bond V^{4+}=O (x0.55) is at 1.64(1) Å, both V^{n+}-O (x4) and V^{n+}-X (x1.25) bonds are at 2.00(1) Å and the V^{4+}--O (x0.20)bonds are at 2.20(1) Å with a common Debye Waller factor of 0.005 Å². The average distances around vanadium obtained from SXRPD and EXAFS are in very good agreement. Indeed, the refinement of the SXRPD pattern of the pristine material leads to an average vanadium-ligands distance of 1.972(6) Å in centrosymmetric vanadium octahedra and for EXAFS, the $<d_{V-L}>_{EXAFS}$ is equal to 1.97(1) Å. The EXAFS model is further supported by the resulting BVS value which is very close to the theoretical one, on the contrary to the one provided from distances calculated from SXRPD (*i.e.* 3.6(1) for EXAFS *vs.* 3.26(1) in average on the two vanadium sites for SXRPD *vs.* 3.55 theoretically). The comparison between distances obtained from SXRPD and EXAFS experiments and associated BVS values are provided in **Table S4**.

During the first step of charge, we found that the oxidation of V^{4+}=O to V^{5+}=O entities occurs without any significant modification of the V-O/F distances along the propagation direction of the chains of octahedra (*i.e.* (i)/(ii), and (i)/(iii)). In the meantime, a significant shortening of the equatorial V-O bonds (*i.e.* (iv)) is observed (from 2.00(1) Å to 1.95(1) Å in average (**Table S4** and **Figure 7**)). The distortion of the PO_4 network compensates for this shortening leading to an enlargement of the Li diffusion channels and thus to the "freezing" of the average cell volume. The values of the average distances obtained from EXAFS are in good agreement with those calculated from SXRPD ($<d_{V-L}>_{SXRPD}$ = 1.96(1) Å and $<d_{V-L}>_{EXAFS}$ = 1.95(1) Å) and, again, the BVS value determined for vanadium in component#2 (i.e. $Li_{0.45}VPO_4F_{0.45}O_{0.55}$) thanks to EXAFS distances (3.9(1) *vs.* 4.10 theoretically) is closer to the theoretical one, versus that calculated from SXRPD distances (*i.e.* 3.65(8)). For component#3, namely $VPO_4F_{0.45}O_{0.55}$, only the bonds belonging to the square plane undergo a significant shortening from 1.95(1)Å to 1.91(1)Å whereas the other ones remain quasi unchanged conferring a BVS value for vanadium of 4.3(1) (instead of 4.55 theoretically).

As illustrated in **Figure 7**, the EXAFS analysis reveals that all along the lithium deintercalation, the competition between the ionicity of the V^{n+}-F bonds and the covalency of the V^{n+}=O bonds constrains the system along the [001] direction related to the vanadyl distortion. Indeed, the (i) V^{n+}=O, (ii) V^{n+}--O and (iii) V^{n+}-F distances don't evolve significantly, in good agreement with XRD. In parallel, the equatorial (iv) V^{n+}-O distances undergo a

significant shortening (about 2.5 %) despite only a tiny contraction of the related cell parameters (i.e. *a* and *b* with variation of 0.05% and 0.18% respectively) is detected by XRD.

Conclusion

Operando XAS experiments conducted during lithium deintercalation from $Li_xVPO_4F_{1-y}O_y$, reveal the activation of the V^{4+}=O/V^{5+}=O redox couple during the first step of the charge and then that of the V^{3+}/V^{4+} redox couple in fluorine rich environment. This result, although surprising, is in full agreement with the experimental operating voltages of the end-member phases, $LiVPO_4F$ and $LiVPO_4O$, and is observed for the first time in the same mixed-valence starting material. Operando SXRPD reveals that the first step corresponds to a wide monophasic domain during which the average structure seems to be frozen. The fit of the EXAFS oscillations has shown that the structural immobilization persists at the local scale for the bond lengths along the propagation direction of the chains of octahedra, and that a shortening of the equatorial V-O distances is observed. This study nicely illustrates the complementarity between *operando* XAS and XRD allowing an in-depth description of crystallographic features combined to that of the electronic states of vanadium in relation with the electrochemical performance. These studies are foreseen to unlock the multi-electron redox in Alkali ion battery cathodes.

Associated Content

* Supporting Information

The Supporting Information is available free of charge on the ACS Publications website via the internet at http://pubs.acs.org. The supporting information gathers all the details of the analyses performed on the Synchrotron X-ray diffraction data and X-ray absorption spectroscopy data, recorded *ex situ* and *in situ* during the cycling of the batteries.

Acknowledgment

The authors thank Rénald David (LRCS) for the synthesis of the $LiVPO_4F_{1-y}O_y$ materials, Thibault Broux (ICMCB/LRCS) for his support with the chemometric analysis, and Tahya Bamine (ICMCB) and Dany Carlier (ICMCB) for fruitful discussions on the local structures observed in these materials. The authors thank also ALBA (Barcelona, Spain) for Synchrotron X-ray diffraction experiments on the MSPD beamline and SOLEIL (Gif-sur-Yvette, France) for

X-ray spectroscopy experiments on the ROCK beamline (financed by the French National Research Agency (ANR) as a part of the "Investissements d'Avenir" program, reference: ANR-10-EQPX-45; proposal number 20160282). The authors also acknowledge FEDER, the Région Hauts-de-France and the RS2E Network for the funding of EB's PhD thesis, as well as the financial support of Région Nouvelle Aquitaine and of the French National Research Agency (STORE-EX Labex Project ANR-10-LABX-76-01 and HIPOLITE Progelec project ANR-12-PRGE-0005-02).

References

(1) Manthiram, A.; Goodenough, J. B. Lithium Insertion into $Fe_2(SO_4)_3$ Frameworks. *J. Power Sources* **1989**, *26*, 403–408.

(2) Masquelier, C.; Croguennec, L. Polyanionic (Phosphates, Silicates, Sulfates) Frameworks as Electrode Materials for Rechargeable Li (or Na) Batteries. *Chem. Rev.* **2013**, *113* (8), 6552–6591.

(3) Ateba Mba, J.M; Masquelier, C.; Suard, E.; Croguennec, L. Synthesis and Crystallographic Study of Homeotypic $LiVPO_4F$ and $LiVPO_4O$. *Chem. Mater.* **2012**, *24*, 1223–1234.

(4) Shi, Y.; Zhou, H.; Seymour, I. D.; Britto, S.; Rana, J.; Wangoh, L. W.; Huang, Y.; Yin, Q.; Reeves, P. J.; Zuba, M.; Chung, Y.; Omenya, F.; Chernova, N.; Zhou, G.; Piper, F.J.; Grey, C.P.; Whittingham, M.S. Electrochemical Performance of Nanosized Disordered $LiVOPO_4$. *ACS Omega* **2018**, *3*, 7310–7323.

(5) Huang, H.; Yin, S.-C.; Nazar, L. F. Approaching Theoretical Capacity of $LiFePO_4$ at Room Temperature at High Rates. *Electrochem. Solid-State Lett.* **2001**, *4* (10), 170–172.

(6) Barker, J.; Gover, R. K. B.; Burns, P.; Bryan, A. A Symmetrical Lithium-Ion Cell Based on Lithium Vanadium Fluorophosphate, $LiVPO_4F$. *Electrochem. Solid-State Lett.* **2005**, *8* (6), 285–287.

(7) Kim, M.; Lee, S.; Kang, B. High Energy Density Polyanion Electrode Material ; $LiVPO_4O_{1-x}F_x$ ($x \approx 0.25$) with Tavorite Structure. *Chem. Mater.* **2017**, *29* (11), 4690–4699.

(8) Boivin, E.; David, R.; Chotard, J. N.; Bamine, T.; Iadecola, A.; Bourgeois, L.; Suard, E.; Fauth, F.; Carlier, D.; Masquelier, C.; Croguennec, L. $LiVPO_4F_{1-y}O_y$ Tavorite-Type Compositions: Influence of the Vanadyl-Type Defects' Concentration on the Structure and Electrochemical Performance. *Chem. Mater.* **2018**, *30* (16), 5682–5693.

(9) Fauth, F.; Peral, I.; Popescu, C.; Knapp, M. The New Material Science Powder Diffraction Beamline at ALBA Synchrotron. *Powder Diffr.* **2013**, *28*, 360–370.

(10) Leriche, J. B.; Hamelet, S.; Shu, J.; Morcrette, M.; Masquelier, C.; Ouvrard, G.; Zerrouki, M.; Soudan, P.; Belin, S.; Elkaïm, E.; et al. An Electrochemical Cell for Operando Study of Lithium Batteries Using Synchrotron Radiation. *J. Electrochem. Soc.* **2010**, *157* (5), 606–610.

(11) Rodriguez-carvajal, J. Recent Advances in Magnetic Structure Determination by Neutron Powder Diffraction. *Phys. B* **1993**, *192*, 55–69.

(12) Briois, V.; La Fontaine, C.; Belin, S.; Barthe, L.; Moreno, T.; Pinty, V.; Carcy, A.; Girardot, R.; Fonda, E. ROCK : The New Quick-EXAFS Beamline at SOLEIL. *J. Phys. Conf. Ser.* **2016**, *712*, 1–6.

(13) Ravel, B.; Newville, M. ATHENA, ARTEMIS, HEPHAESTUS: Data Analysis for X-Ray Absorption Spectroscopy Using IFEFFIT. *J. Synchrotron Radiat.* **2005**, *12*, 537–541.

(14) Jaumot, J.; de Juan, A.; Tauler, R. MCR-ALS GUI 2.0: New Features and Applications. *Chemom. Intell. Lab. Syst.* **2015**, *140*, 1–12.

(15) Jaumot, J.; Gargallo, R.; Juan, A.; Tauler, R. A Graphical User-Friendly Interface for MCR-ALS: A New Tool for Multivariate Curve Resolution in MATLAB. *Chemom. Intell. Lab. Syst.* **2005**, *76*, 101–110.

(16) Ateba Mba, J. M.; Croguennec, L.; Basir, I.; Barker, J.; Masquelier, C. Lithium Insertion or Extraction from / into Tavorite-Type $LiVPO_4F$: An In Situ X-Ray Diffraction Study. *J. Electrochem. Soc. Soc.* **2012**, *159* (8), 1171–1175.

(17) Bianchini, M.; Ateba-Mba, J. M.; Dagault, P.; Bogdan, E.; Carlier, D.; Suard, E.; Masquelier, C.; Croguennec, L. Multiple Phases in the ε-VPO_4O–$LiVPO_4O$–Li_2VPO_4O System: A Combined Solid State Electrochemistry and Diffraction Structural Study. *J. Mater. Chem. A* **2014**, *2*, 10182–10192.
(18) Ellis, B. L.; Ramesh, T. N.; Davis, L. J. M.; Goward, G. R.; Nazar, L. F. Structure and Electrochemistry of Two-Electron Redox Couples in Lithium Metal Fluorophosphates Based on the Tavorite Structure. *Chem. Mater.* **2011**, *23*, 5138–5148.
(19) Boivin, E. PhD Thesis: Crystal Chemistry of Vanadium Phosphates as Positive Electrode Materials for Li-Ion and Na-Ion Batteries, University of Picardie Jules Verne, 2017.
(20) Broux, T.; Bamine, T.; Simonelli, L.; Stievano, L.; Fauth, F.; Ménétrier, M.; Carlier, D.; Masquelier, C.; Croguennec, L. V^{IV} Disproportionation Upon Sodium Extraction From $Na_3V_2(PO_4)_2F_3$ Observed by Operando X-Ray Absorption Spectroscopy and Solid State NMR. *J. Phys. Chem. C* **2017**, *121*, 4103–4111.
(21) Fehse, M.; Iadecola, A.; Sougrati, M. T.; Conti, P.; Giorgetti, M.; Stievano, L. Applying Chemometrics to Study Battery Materials: Towards the Comprehensive Analysis of Complex Operando Datasets. *Energy Storage Mater.* **2019**, *18*, 328–337.